Purdue University
Purdue e-Pubs

Birck and NCN Publications | Birck Nanotechnology Center

8-2010

Loss-free and active optical negative-index metamaterials

Shumin Xiao
Purdue University, xiao2@purdue.edu

V. P. Drachev
Birck Nanotechnology Center, School of Electrical and Computer Engineering, Purdue University, vdrachev@purdue.edu

Alexander V. Kildishev
Birck Nanotechnology Center, School of ECE, kildishev@purdue.edu

Xingjie Ni
Purdue University - Main Campus, xni@purdue.edu

Uday K. Chettiar
Purdue University, uday@purdue.edu

See next page for additional authors

Follow this and additional works at: http://docs.lib.purdue.edu/nanopub

Part of the Nanoscience and Nanotechnology Commons

Xiao, Shumin; Drachev, V. P.; Kildishev, Alexander V.; Ni, Xingjie; Chettiar, Uday K.; Yuan, Hsiao-Kuan; and Shalaev, V. M., "Loss-free and active optical negative-index metamaterials" (2010). *Birck and NCN Publications.* Paper 701.
http://dx.doi.org/10.1038/nature09278

This document has been made available through Purdue e-Pubs, a service of the Purdue University Libraries. Please contact epubs@purdue.edu for additional information.

Authors
Shumin Xiao, V. P. Drachev, Alexander V. Kildishev, Xingjie Ni, Uday K. Chettiar, Hsiao-Kuan Yuan, and V. M. Shalaev

This article is available at Purdue e-Pubs: http://docs.lib.purdue.edu/nanopub/701

LETTERS

Loss-free and active optical negative-index metamaterials

Shumin Xiao[1], Vladimir P. Drachev[1], Alexander V. Kildishev[1], Xingjie Ni[1], Uday K. Chettiar[1]†, Hsiao-Kuan Yuan[1]† & Vladimir M. Shalaev[1]

The recently emerged fields of metamaterials and transformation optics promise a family of exciting applications such as invisibility, optical imaging with deeply subwavelength resolution and nanophotonics with the potential for much faster information processing. The possibility of creating optical negative-index metamaterials (NIMs) using nanostructured metal–dielectric composites has triggered intense basic and applied research over the past several years[1–10]. However, the performance of all NIM applications is significantly limited by the inherent and strong energy dissipation in metals, especially in the near-infrared and visible wavelength ranges[11,12]. Generally the losses are orders of magnitude too large for the proposed applications, and the reduction of losses with optimized designs seems to be out of reach. One way of addressing this issue is to incorporate gain media into NIM designs[13–16]. However, whether NIMs with low loss can be achieved has been the subject of theoretical debate[17,18]. Here we experimentally demonstrate that the incorporation of gain material in the high-local-field areas of a metamaterial makes it possible to fabricate an extremely low-loss and active optical NIM. The original loss-limited negative refractive index and the figure of merit (FOM) of the device have been drastically improved with loss compensation in the visible wavelength range between 722 and 738 nm. In this range, the NIM becomes active such that the sum of the light intensities in transmission and reflection exceeds the intensity of the incident beam. At a wavelength of 737 nm, the negative refractive index improves from −0.66 to −1.017 and the FOM increases from 1 to 26. At 738 nm, the FOM is expected to become macroscopically large, of the order of 10^6. This study demonstrates the possibility of fabricating an optical negative-index metamaterial that is not limited by the inherent loss in its metal constituent.

Optical NIMs are artificially tailored composites where a counter-intuitive negative refractive index arises from the nanoscale 'meta-atoms' designed into the material. These optical NIM building blocks typically require a plasmonic material such as silver or gold in addition to dielectric constituents. Losses inherent in these noble metals at optical frequencies plague the entire field of metamaterials and are one of the major restrictions preventing metamaterials from leaving the domain of academic research and entering industrial applications. Recently, the incorporation of an active material has been suggested as a viable and effective method of minimizing or eliminating loss in NIMs[13–16]. This method has been theoretically discussed in a variety of gain models, resulting in predictions of drastic performance improvements[19–22]. However, the high levels of gain required for this method were previously considered impossible to obtain in experiments[23,24]. The impairment of low gain levels can be overcome by using a thick active host layer, as was shown in the recent demonstration of the spaser[21,25,26]. However, in a NIM-based device the thickness of the active material must necessarily be kept small to preserve the negative refractive index. The incorporation of gain in an optical NIM design has been hampered by these difficulties, but such an achievement would lead to the production of low- or no-loss optical NIMs for use in a large number of breakthrough applications.

We have overcome this limitation by an approach in which the active medium within the NIM gives rise to an effective gain much higher than its bulk counterpart. The large value of gain is due to the local-field enhancement inherent in the plasmonic response of NIMs[20,22], a phenomenon that provides a new direction for the compensation of losses in NIMs. In our experiments, the transmission through the optical NIM sample is amplified by pumping the active medium within it, and the structure is carefully designed such that the active medium experiences the highest local field while preserving the negative-index property of the metamaterial. Our experimental results, along with our numerical simulations, directly demonstrate that our NIM sample is lossless and active.

The NIM structure in our experiment is the fishnet structure, which was also used in some of the earliest demonstrations of optical NIMs[7,27]. Epoxy doped with rhodamine 800 (Rh800) dye is used as the gain medium. The fabrication process for creating the gain-assisted fishnet sample is schematically shown in Fig. 1 (see Methods for details). In this proposed structure, the typical alumina spacer of the initial fishnet structure is replaced by the gain medium. Successful fabrication is extremely challenging because the nanostructure can be easily destroyed during this critical replacement process. The scanning electron microscope (SEM) images of the structure at different fabrication steps (Fig. 2; see Methods for details) indicate that no damage to our fishnet structure occurred during this process.

The fabricated sample was first optically characterized by means of far-field transmission and reflection measurements, using normally incident light at the primary polarization with the electric field vector of the light along the x axis in Fig. 2a (Methods). The blue, red and green solid lines in Fig. 3a represent the transmission, reflection and absorptance spectra of the sample, respectively. A clear resonance around 725 nm can be observed, which matches very well with the fluorescence peak of Rh800. Here the low transmission is solely due to high absorption because the impedance of the sample is nearly matched and, hence, the reflection is low around the resonance. By applying a Lorentz-oscillator absorption model for the material properties of the Rh800–epoxy combination, the experimental spectra were matched well with numerical simulations (dotted lines in Fig. 3a), and the effective permittivity and permeability of the sample were determined following the bianisotropic parameter retrieval

[1]Birck Nanotechnology Center and School of Electrical and Computer Engineering, Purdue University, West Lafayette, Indiana 47907, USA. †Present addresses: Department of Electrical and Systems Engineering, University of Pennsylvania, 200 South 33rd St, Philadelphia, Pennsylvania 19104, USA (U.K.C.); Intel, 2501 NW 229th Avenue, RA2-283, Hillsboro, Oregon 97124, USA (H.-K.Y.).

©2010 Macmillan Publishers Limited. All rights reserved

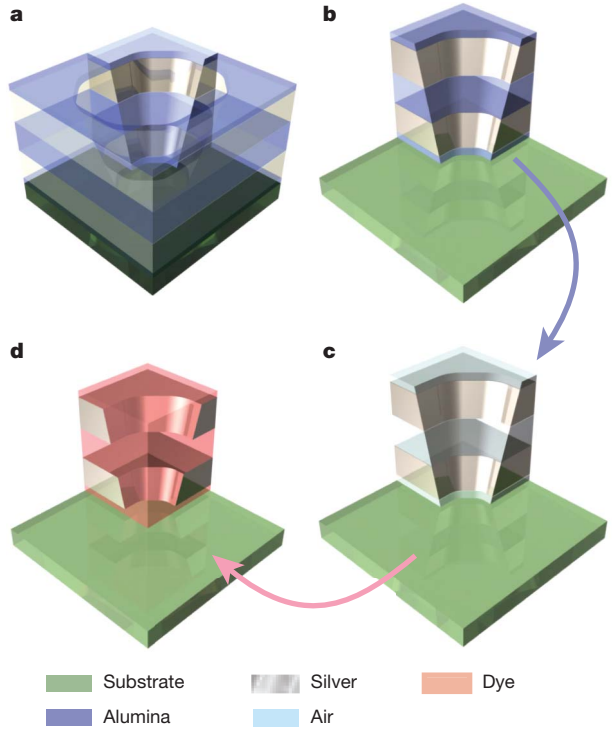

Figure 1 | Schematic of the fabrication process. **a**, Unit cell of the fishnet structure with alumina as the spacer material between two silver layers. **b**, One-quarter of the fishnet structure with an alumina spacer. **c**, After etching the alumina, the fishnet structure has air or solvent as the spacer with alumina pillars as support. **d**, After coating with Rh800–epoxy, the fishnet structure has the dye–epoxy material in the spacer region and above the fishnet structure.

method described in ref. 28. A negative refractive index was obtained from 720 to 760 nm, with the strongest negative index, of $n' = -0.86$, occurring at 740 nm. The maximum FOM (FOM $= -n'/|n''|$, for $n' < 0$, where n' and n'' are respectively the real and imaginary parts of the refractive index) was 1 at 737 nm.

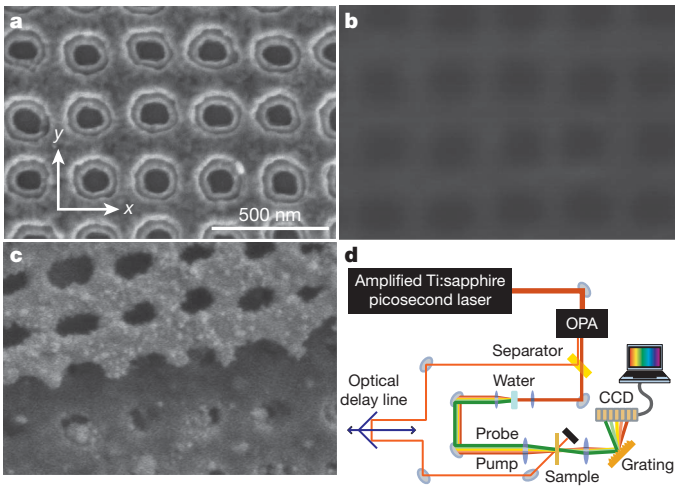

Figure 2 | SEM images of the fishnet structure at different fabrication stages. **a**, Fishnet structure with alumina spacer. **b**, After etching the alumina and coating with Rh800–epoxy, the fishnet structure has the dye–polymer as the spacer and on the top. **c**, Tilt-view SEM image of the structure after coating with Rh800–epoxy and after a part of the top layer of silver has been removed by focused ion-beam milling. The scale is the same in all of the SEM images. **d**, The pump–probe experimental set-up. CCD, charge-coupled device; OPA, optical parametric amplifier.

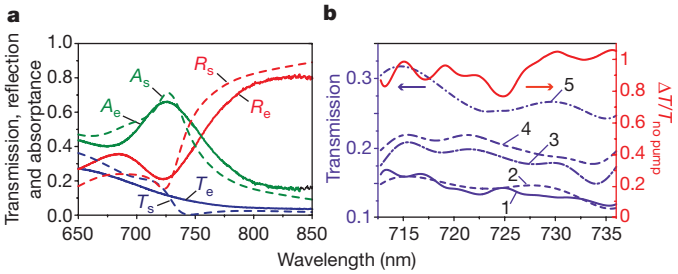

Figure 3 | Experimental results and simulation. **a**, Experimental far-field transmission (T_e), reflection (R_e) and absorptance (A_e) spectra of the sample, along with simulated results (T_s, R_s, and A_s) at the primary linear polarization shown in Fig. 2a. **b**, The transmission spectra without pumping (line 1), with the optimized delay between pump and probe (probe pulse is 54 ps later than the pump) and 1-mW pumping power (line 5), with the optimized delay and 0.12-mW pumping power (line 3), with the optimized delay and 0.16-mW pumping power (line 4), and with the pump preceding the probe by 6 ps and 1-mW pumping power (line 2). The wavelength-dependent relative transmission change from the pump–probe experiment is shown by the red solid line.

The compensation of loss in the structure was investigated with a pump–probe experiment. The experimental set-up is shown in Fig. 2d and explained in detail in Methods. The polarizations of the pump and probe pulses were both along the primary polarization. The results of the pump–probe measurements are shown in Fig. 3b. We first measured the transmission spectrum without pumping (blue line 1 in Fig. 3b). The unpumped transmission value is nearly the same as that given by the blue solid line in Fig. 3a in the same wavelength region, and confirms the validity of the measurement. We then measured the transmission of the sample with the pump laser turned on and the average power fixed at 1 mW, which is below the damage threshold for the sample but five times larger than the gain saturation power for Rh800–epoxy. We optimized the delay time between the pump and probe pulses to ensure that the dye offered the maximum gain. The transmission spectrum increased significantly when the gain medium was pumped (blue line 5 in Fig. 3b). The relative change between the transmission values with and without pumping ($\Delta T/T_{\mathrm{nopump}}$, where $\Delta T = T_{\mathrm{pump}} - T_{\mathrm{nopump}}$) is plotted as the red line in Fig. 3b. The transmission was enhanced by about 100% within a wide wavelength range from 712 to 736 nm. These measurements far exceed the experimental error, which was less than 10%. To exclude the possibility of damage-induced transparency, the measurements with and without pumping were repeated ten times. We note that, under the conditions of our experiment (average power, 1 mW; repetition rate, 1 kHz), photobleaching was observed after 5 min of illumination. We also measured the transmission spectrum of the sample with a different (non-optimal) delay by tuning the probe beam pulse to be 6 ps earlier than the pump pulse (blue line 2 in Fig. 3b), and compared this result with the unpumped spectrum. This detuned spectrum matches the spectrum without pumping very well, indicating that influences from the set-up and local heating can be excluded from our results.

Another control experiment on a similar sample with pure epoxy as the spacer shows no changes in the transmission in any measurements. Therefore, we conclude that the changes in transmission observed from the Rh800–epoxy sample are caused by the compensation of loss in the metamaterial. We also performed the pump–probe experiment with an optimized delay time between the pump and probe pulses at lower pump intensities. The results are plotted as blue lines 3 and 4 in Fig. 3b. Under the much lower pumping intensity, the pumping does not result in the required population inversion in the dye molecules and thus does not offer the needed gain; instead, it only reduces the absorption of the dye, such that the transmission change is much smaller in this case.

The loss compensation mechanism in the sample is relatively straightforward to understand. When Rh800 is excited by a pump

©2010 Macmillan Publishers Limited. All rights reserved

pulse with sufficiently high power, a population inversion is formed inside the dye molecules. This provides amplification for a properly delayed probe pulse whose wavelength is coincident with the stimulated emission wavelength of the dye molecules. As a result of this amplification, the transmission of the probe light through the sample increases. Once the pump is turned off or the probe pulse is detuned away from the optimal delay value, the probe light no longer experiences amplification during its propagation through the device, and the transmission drops back down to its initial (unpumped) value.

We performed numerical simulations to understand the effects of gain on the corresponding transmission spectra and to determine the refractive index and FOM of the gain-assisted sample (Methods). In Supplementary Fig. 2, we show how the relative transmission through the sample depends on the effective gain value, g_{sim}. When g_{sim} increases, the transmission through the sample also increases. For $g_{sim} = 2{,}800\ cm^{-1}$ around 725 nm (the centre wavelength of the fluorescence of Rh800), the simulated relative change between transmission with and without gain matches our experimental result well (Fig. 3b). The value of g_{sim} in our simulations is about seven times larger than that measured for a homogeneous slab of dye-doped epoxy, which could be due to a chemical enhancement mechanism known to have an important role, for example, in surface-enhanced Raman scattering[29]. Another possible reason for such an increase in gain could be related to a feedback mechanism analogous to that occurring in a spaser[25]. We also note that similar gain values for dye molecules were reported by other groups in experiments on the compensation of losses in surface plasmons[23].

With a change in the refractive index accompanying the loss compensation, the impedances at the interface between the sample and air become mismatched and, thus, the spectral reflection also increases with gain, reaching 107.6% at 730 nm. The sum of the field intensities in transmission and reflection is nearly 1.23 times larger than the intensity of the incident beam at this wavelength. This confirms that the incident light is indeed amplified in the sample such that the absorptance, A, is negative and the sample is active. According to Fig. 4a, the NIM remains active within a spectral range between 722 and 738 nm, and the refractive index is negative in a broader range, between 720 and 760 nm.

The effective refractive index and FOM were determined from the simulated spectra and are shown in Fig. 4 (for details of our bianisotropic parameter retrieval, see Methods). The real part of the refractive index, n', becomes more negative after gain is applied, and the imaginary part, n'', also drops significantly near the resonance. At 737 nm, n' changes with the addition of gain from -0.66 to -1.017, whereas n'' decreases from 0.66 to 0.039 (Fig. 4b). This corresponds to an increase in FOM from 1 to 26, as seen in Fig. 4c. This value is so far the largest reported FOM achieved in any NIM in the optical region; it is much larger even than the values reported for two-dimensional metamaterial waveguides[30]. An even larger FOM is expected to be achieved at 738 nm, where it should be of the order of 10^6 ($n' = -1.26$, $n'' = 1 \times 10^{-6}$), and the structure is practically loss free ($A \leq 0$), even at macroscopically large sizes. Although experimentally it is hard to tune the gain and other parameters exactly to the optimized performance point, it is still easy to achieve FOM values close to 10^2 within about a 3-nm wavelength range near the resonance. We note that with a further increase in gain, n'' for our sample does not become negative but instead starts to increase. This occurs because the impedance mismatch grows at this level of gain, leading to increased front-side reflection and asymmetry in the front- and back-side reflections. The NIM remains active with $A < 0$ in a relatively broad range between 722 and 738 nm. We believe that by further improving the structure's design, it is possible to obtain a NIM with a macroscopically large FOM in a much broader spectral range. We also note that the use of the standard definition of FOM ($-n'/|n''|$, for $n' < 0$) is normally reserved for non-bianisotropic metamaterials, because in bianisotropic ones the losses depend on the bianisotropy parameters; hence, the ratio $-n'/|n''|$ becomes less useful in quantifying the loss in bianisotropic NIMs. In that sense, the most important finding here is related to the presence of a region where $A < 0$ and $n' < 0$.

The loss compensation also produces drastic changes in the effective dielectric permittivity and magnetic permeability of the sample. Figure 4d shows the effective real parts of the permittivity, ε', and the permeability, μ', for the sample with and without gain. Owing to a stronger electric resonance along with a stronger magnetic antiresonance achieved with gain, ε' and μ' both become narrower, in agreement with theoretical considerations[22].

The effectiveness of the loss compensation in our sample arises from the local-field enhancement of the structure when a gain medium is used as the spacer layer[20,22]. Because the effective extinction coefficients at 737 nm are $\alpha \approx 6.75 \times 10^3\ cm^{-1}$ and $\alpha \approx 1.13 \times 10^5\ cm^{-1}$ for the device with and without gain, respectively, the effective amplification is $\alpha \approx -1.07 \times 10^5\ cm^{-1}$, which is 46 times larger at this wavelength than the 'seed' value (without the local-field factor) that was used in simulations. According to our numerical modelling, the high local fields in the fishnet structure result in a total (spatially integrated) energy produced by the gain medium that is about 45 times larger than that produced by a homogeneous gain material of the same volume, in good agreement with the factor of 46 found above (Methods).

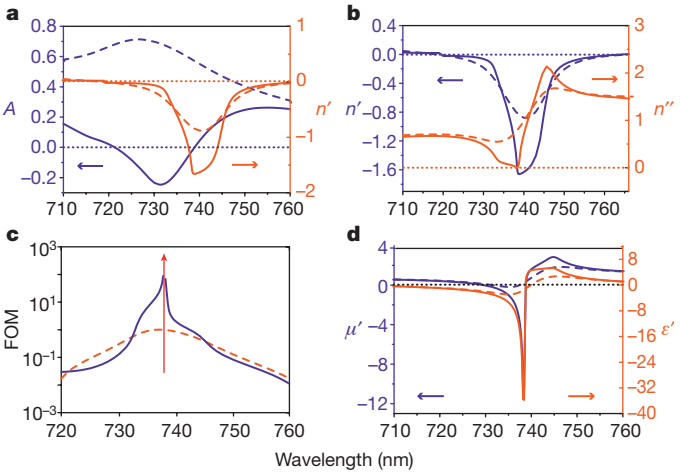

Figure 4 | Simulation and determined parameters. **a**, The simulated refractive index, n' (real part), and absorptance, A (in the forward direction), as functions of wavelength with (solid) and without (dashed) gain. **b**, The effective refractive index, $n = n' + in''$, determined with (solid) and without (dashed) gain. **c**, The effective FOM determined with (solid) and without (dashed) gain (the FOM is set to zero when the real part of the refractive index is positive). **d**, The effective permittivity, ε' (real part), and permeability, μ' (real part), determined with (solid) and without (dashed) gain.

METHODS SUMMARY

Fabrication of the fishnet structure with a gain medium as the spacer is accomplished by a post-processing method. First we fabricate the fishnet sample with Al_2O_3 as a spacer using standard electron-beam lithography with a Leica VB6 writer and lift-off processes. Then chemical etching is used to remove the Al_2O_3 spacer and, finally, epoxy with dye molecules is used to fill the vacated space.

Far-field measurements for transmission and reflection of the fishnet with Rh800–epoxy as the spacer are performed and used to determine the effective parameters without pumping. We measure the transmission for the gain-assisted fishnet by using a pump–probe set-up at three different pump levels; the gain line shape of the Rh800–epoxy is obtained with a pump energy above the saturation energy.

In the numerical studies of the gain-assisted fishnet metamaterial, the intrinsic losses of the metal are included. The loss is increased by a factor of about three relative to that of bulk silver to account for the additional loss resulting from electron scattering in the fabricated nanostructures. Without the pump, the Rh800–epoxy material is described by the dielectric function $\varepsilon_p(\lambda) = 1.65^2 + i\varepsilon''(\lambda)$, where $\varepsilon''(\lambda)$ is the loss line shape obtained from experiments with no pumping.

©2010 Macmillan Publishers Limited. All rights reserved

Full Methods and any associated references are available in the online version of the paper at www.nature.com/nature.

Received 14 December 2009; accepted 14 June 2010.

1. Veselago, V. G. The electrodynamics of substances with simultaneously negative value of ε and μ. *Sov. Phys. Usp.* **10,** 509–514 (1968).
2. Pendry, J. B. Negative refractive makes a perfect lens. *Phys. Rev. Lett.* **85,** 3966–3969 (2000).
3. Shalaev, V. M, *et al.* Negative index of refraction in optical metamaterials. *Opt. Lett.* **30,** 3356–3358 (2005).
4. Pendry, J. B., Schurig, D. & Smith, D. R. Controlling electromagnetic fields. *Science* **312,** 1780–1782 (2006).
5. Soukoulis, C. M., Linden, S. & Wegener, M. Negative refractive index at optical wavelengths. *Science* **315,** 47–49 (2007).
6. Valentine, J. *et al.* Three-dimensional optical metamaterial with a negative refractive index. *Nature* **455,** 376–379 (2008).
7. Zhang, S, *et al.* Experimental demonstration of near-infrared negative-index metamaterials. *Phys. Rev. Lett.* **95,** 137404 (2005).
8. Shalaev, V. M. Optical negative-index metamaterials. *Nature Photon.* **1,** 41–48 (2006).
9. Tsakmakidis, K. L., Boardman, A. D. & Hess, O. 'Trapped rainbow' storage of light in metamaterials. *Nature* **450,** 397–401 (2007).
10. Kildishev, A. V. & Shalaev, V. M. Engineering space for light via transformation optics. *Opt. Lett.* **33,** 43–45 (2008).
11. Pinchuk, A., Kreibig, U. & Hilger, A. Optical properties of metallic nanoparticles: influence of interface effects and interband transitions. *Surf. Sci.* **557,** 269–280 (2004).
12. Drachev, V. P. *et al.* The Ag dielectric function in plasmonic metamaterials. *Opt. Exp.* **16,** 1186–1195 (2008).
13. Noginov, M. A. *et al.* Enhancement of surface plasmons in an Ag aggregate by optical gain in a dielectric medium. *Opt. Lett.* **31,** 3022–3024 (2006).
14. Ramakrishna, S. A. & Pendry, J. B. Removal of absorption and increase in resolution in a near-field lens via optical gain. *Phys. Rev. B* **67,** 201101 (2003).
15. Klar, T. A., Kildisher, A. V., Drachev, V. P. & Shalaev, V. M. Negative-index metamaterial: going optical. *IEEE J. Sel. Top. Quantum Electron.* **12,** 1106–1115 (2006).
16. Sarychev, A. K. & Tartakovsky, G. Magnetic plasmonic metamaterials in actively pumped host medium and plasmonic nanolaser. *Phys. Rev. B* **75,** 085436 (2007).
17. Stockman, M. I. Criterion for negative refraction with low optical losses from a fundamental principle of causality. *Phys. Rev. Lett.* **98,** 177404 (2007).
18. Kinsler, P. & McCall, M. W. Causality-based criteria for a negative refractive index must be used with care. *Phys. Rev. Lett.* **101,** 167401 (2008).
19. Wegener, M. *et al.* Toy model for plasmonic metamaterial resonances coupled to two-level system gain. *Opt. Exp.* **16,** 19785–19788 (2008).
20. Fang, A., Koschny, Th., Wegener, M. & Soukoulis, C. M. Self-consistent calculation of metamaterial with gain. *Phys. Rev. B* **79,** 241104 (2009).
21. Zheludev, N. I., Prosvirnin, S. L., Papasimakis, N. & Fedotov, V. A. Lasing spaser. *Nature Photon.* **2,** 351–354 (2008).
22. Sivan, Y., Xiao, S., Chettiar, U. K., Kildishev, A. V. & Shalaev, V. M. Frequency-domain simulations of a negative-index material with embedded gain. *Opt. Exp.* **26,** 24060–24074 (2009).
23. Noginov, M. A. *et al.* Compensation of loss in propagating surface plasmon polariton by gain in adjacent dielectric media. *Opt. Exp.* **16,** 1385–1392 (2008).
24. Klimov, V. I. *et al.* Optical gain and stimulated emission in nanocrystal quantum dots. *Science* **290,** 314–317 (2000).
25. Stockman, M. I. The spaser as a nanoscale quantum generator and ultrafast amplifier. *J. Opt.* **12,** 024004 (2010).
26. Plum, E., Fedotov, V. A., Kuo, P., Tsai, D. P. & Zheludev, N. I. Towards the lasing spaser: controlling metamaterial optical response with semiconductor quantum dots. *Opt. Exp.* **17,** 8548–8551 (2009).
27. Xiao, S. *et al.* Yellow-light negative-index metamaterials. *Opt. Lett.* **34,** 3478–3480 (2009).
28. Kriegler, C. E., Rill, M. S., Linden, S. & Wegener, M. Bianisotropic photonic metamaterials. *IEEE J. Sel. Top. Quantum Electron.* **16,** 367–375 (2010).
29. Fromm, D. P. *et al.* Exploring the chemical enhancement for surface-enhanced Raman scattering with Au bowtie nanoantennas. *J. Chem. Phys.* **124,** 061101 (2006).
30. Lezec, H. J., Dionne, J. A. & Atwater, H. A. Negative refraction at visible frequencies. *Science* **316,** 430–432 (2007).

Supplementary Information is linked to the online version of the paper at www.nature.com/nature.

Acknowledgements This work was supported in part by ARO-MURI awards 50342-PH-MUR and W911NF-09-1-0539 and by NSF PREM grant no. DMR 0611430. The authors acknowledge valuable discussions with T. Klar. V.M.S. is grateful to Y. Sivan and Z. Jacob for their comments.

Author Contributions S.X. fabricated the samples and conducted optical characterization and part of the numerical simulations; S.X. and V.P.D. assembled the set-up; V.P.D. guided the optical experiments and partly the numerical simulations and fabrication; A.V.K. guided the numerical simulations and developed a sample-specific analytical technique for retrieving the bianisotropic parameters; A.V.K. and X.N. performed numerical simulations; U.K.C. performed part of the numerical simulations and implemented parallelism in the design and retrieval optimization; H.-K.Y. suggested and developed the original fabrication approach; S.X., V.P.D., A.V.K., X.N. and V.M.S. wrote the manuscript; V.M.S. led the project and discussed the fabrication, optical characterization and numerical modelling.

Author Information Reprints and permissions information is available at www.nature.com/reprints. The authors declare no competing financial interests. Readers are welcome to comment on the online version of this article at www.nature.com/nature. Correspondence and requests for materials should be addressed to V.M.S. (shalaev@purdue.edu).

©2010 **Macmillan Publishers Limited. All rights reserved**

METHODS

Fabrication methods. To obtain the maximum usefulness of our gain medium, the alumina spacer of our fishnet structure was replaced with the selected dye–epoxy material. This places the dye–epoxy in the region of highest local fields and thus maximizes the overall gain. The main restriction in fabrication is the possibility of the fishnet structure collapsing and being damaged during the etching process to remove the alumina spacer. Once such damage occurs, the negative index of the metamaterial disappears and is unrecoverable. In our experiment, we first fabricated an $80 \times 80\ \mu m^2$ fishnet sample on a 15-nm-thick indium tin oxide (ITO)-coated glass substrate. The vertical structure consists of a 50-nm alumina layer sandwiched by two 50-nm perforated silver layers, which are protected by 10-nm alumina layers both at the top and bottom surfaces. The in-plane fishnet structure is shown in Fig. 2a, where the geometry is defined by 280-nm periodicity in both lateral directions. The widths of the fishnet nanostrips are 163 nm in the x direction and 207 nm in the y direction.

Next the alumina is etched in tetramethylammonium hydroxide solution. The etching time is precisely controlled to create thin alumina pillars between the perforated metal layers. The pillars are significantly smaller than the fishnet nanostrips. Therefore, collapse of, and damage to, the fishnet structure can be avoided and enough space is left for the gain material. Then a 800-nm epoxy film doped with Rh800 at a concentration of 2×10^{-2} M is spin-coated onto the sample. Rh800 is selected here because of its relatively high quantum efficiency and high solubility in the organic host. The concentration of Rh800 molecules in the epoxy film is $1.2 \times 10^{19}\ cm^{-3}$, and the measured spectral absorption and emission peaks of Rh800 in epoxy are at 690 nm and 724 nm, respectively. During the spin-coating process, the Rh800–epoxy solution penetrates into the fishnet holes and fills the voids left by the etched spacer layer. Finally, reactive ion etching is used to etch the thickness of the Rh800–epoxy layer down to 220 nm, leaving only about 60 nm on top of the fishnet structure. Figure 2b shows the SEM image of the polymer-coated fishnet structure. Although the structure is almost indiscernible owing to the Rh800–epoxy layer covering the fishnet surface, the profile of the fishnet structure can still be seen. To confirm that our fishnet structures are damage free after the fabrication process, we removed the epoxy layer and the top layer of silver by focused ion-beam milling. Figure 2c in the paper shows the tilt-view SEM image of the top layer of the structure after such milling. The clean and undamaged silver fishnet can be observed, showing no cracks, collapse or other defects.

Far-field measurement. The set-up used for far-field measurement is shown and described in detail in our previous paper[31]. As our measurements showed, the secondary polarization (with the electric field vector of the incident light along the y axis in Fig. 2a) shows a weak resonance around 780 nm. This polarization was not used in our pump–probe experiments because, as follows from the numerical simulation and retrieved results, it does not exhibit a negative refractive index at the resonance, and the resonance is far away from the strong-emission region of the gain. Thus, all the pump-probe results are shown for the primary polarization.

Pump–probe measurement. A 690-nm incident beam from an optical parametric amplifier pumped by an 800-nm, picosecond Ti:sapphire laser is focused onto the sample and acts as the pump beam. The spot size is 200 μm. A supercontinuum, white-light source generated by pumping water with an 800-nm pulse from the laser is normally focused to a 70-μm spot on the sample as a probe beam. The probe beam is sent at a very small angle with respect to the pump beam, providing a good overlap of the two beams on the sample surface. The pulse duration and repetition rate of both beams are 2 ps and 1 kHz, respectively. The time delay between the two beams is adjusted by an optical delay line, which gives us a time resolution of 6 ps. The optimum time delay between the probe and pump pulses is about 54 ps; this delay provides the maximum amplification of the probe beam. The transmission of the probe light is then collected from a 30–40-μm spot at the centre of the fishnet structure and analysed with a spectrometer with an acquisition time of 15 s. We focused our study on the spectral region near the luminescence peak wavelength of the Rh800 dye by exploiting the full spectral range of the grating/CCD detection. The angular position of the grating remained unchanged.

Numerical simulations. The numerical simulations of the sample were performed with the COMSOL MULTIPHYSICS software package. In simulations, we used the dispersive dielectric function for ITO,

$$\varepsilon_{ITO} = 4 - \left(\frac{\lambda}{597.6}\right)^2 \left(1 + \frac{i\lambda}{16067.6}\right)^{-1}$$

For the active gain medium, the gain is taken into account in the imaginary part of the refractive index of the Rh800–epoxy material; hence, the refractive index of the Rh800–epoxy material is defined as $n_a(\lambda) = 1.65 - i(100/4\pi)\lambda g_{sim}(\lambda)$, where $g_{sim}(\lambda)$ is the gain line shape obtained from the experiment with a constant pump (Supplementary Fig. 1). In contrast to the active gain medium, the passive regime is implemented by using the dielectric function $\varepsilon_p(\lambda) = 1.65^2 + i\varepsilon''(\lambda)$, where $\varepsilon''(\lambda)$ is the loss line shape obtained from the experiment with no pump.

In retrieving the effective parameters of a sample, the trapezoidal cross-section and the substrate effect in fishnet-type NIMs can induce non-zero effective bianisotropy parameters[32]. To retrieve the effective parameters accurately, a bianisotropic retrieval method is used. Similar to the approach shown in ref. 28, we use a technique built on the transfer matrix

$$t = \begin{pmatrix} t_{11} & t_{12} \\ t_{21} & t_{22} \end{pmatrix} = {t_3}^{-1} {z_4}^{-1} \begin{pmatrix} t_+ & r_- + 1 \\ t_+ & r_- - 1 \end{pmatrix} \begin{pmatrix} 1 + r_+ & t_- \\ 1 - r_+ & -t_- \end{pmatrix}^{-1} \quad (1)$$

where r_+ is the complex reflection coefficient computed at the air–epoxy interface and t_+ is the complex transmission coefficient obtained at the ITO–glass interface upon structure-side illumination. The component r_- is the complex reflection coefficient computed at the ITO–glass interface and t_- is the complex transmission coefficient obtained at the air–epoxy interface on substrate-side illumination. Also, $z_4 = \mathrm{diag}(1,\ {n_{SUB}}^{-1})$, $n_{SUB} = 1.52$, $t_3 = (1/2){z_3}^{-1} u s_3(\delta_{ITO}) u z_3$, $\delta_{ITO} = 15$ nm, $z_3 = \mathrm{diag}(1,\ {n_{ITO}}^{-1})$, n_{ITO} is the wavelength-dependent refractive index of the ITO layer, $s_3(x) = \mathrm{diag}(e^{ik_0 n_{ITO} x}, e^{-ik_0 n_{ITO} x})$, k_0 is the vacuum wavevector and

$$u = \begin{pmatrix} 1 & 1 \\ 1 & -1 \end{pmatrix}$$

In equation (1) we have used the identity $t_- = t_+ n_{SUB}$, because the structure is reciprocal.

Then, using the factorization of t and the substitutions $\sigma = t_{11} + t_{22}$, $\delta = t_{11} - t_{22}$, $\Delta = \pm\sqrt{\delta^2 + \tau^2}$, $\tau^2 = 4t_{12}t_{21}$ and $s_\pm = (\sigma \mp \Delta)/2$, we finally obtain the effective parameters of the bianisotropic slab as

$$n = (k_0 x_0)^{-1} \cos^{-1}(\sigma/2)$$

$$z_\pm = (\pm\delta - \Delta)/2t_{21}$$

where x_0 is the thickness of the slab.

Once the values of n, z_+ and z_- are known, the effective parameters ε, μ and ξ are retrieved using the formulae

$$\varepsilon = 2n/(z_+ + z_-)$$

$$\xi = i\varepsilon(z_- - z_+)/2 = in\delta/\Delta$$

$$\mu = (n^2 - \xi^2)/\varepsilon$$

which are consistent with ref. 28.

An alternative method of validating our retrieval procedure, which is built on the classical Kramers–Kronig relation[33,34], has been applied to the available (truncated) spectral range. The Kramers–Kronig relation for the refractive index links the frequency-dependent n' and n'' expressions through the principal value of the integral

$$n'(v) = 1 - \frac{2}{\pi} \int_{\omega_1}^{\omega_2} \omega n''(\omega)(\omega^2 - v^2)^{-1}\, d\omega$$

Here ω_1 and ω_2 are the integral's low- and high-frequency limits. We have directly used a numerical integration scheme using the subgrid midpoints $v_l = (\omega_l + \omega_{l+1})/2$ obtained from the initially non-uniform spectral grid ω. Thus, the values of $n_l' = n'(v_l)$ are calculated using

$$n_l' = 1 - \frac{1}{\pi} \sum_1^{p_{max}-1} \Delta\omega_p \left[\frac{\omega_{p+1} n''_{p+1}}{\omega_{p+1}^2 - v_l^2} + \frac{\omega_p n''_p}{\omega_p^2 - v_l^2}\right]$$

with $\Delta\omega_p = \omega_{p+1} - \omega_p$ and $n_p'' = n''(\omega_p)$. Supplementary Fig. 3 compares the values for n'' obtained with the truncated Kramers–Kronig numerical convolution (red line with squares) with the n'' values retrieved with our general scheme based on refs 28, 35 (black line). Although there is some expected mismatch at the edges, which is due to the truncation of the spectral range, the figure indicates sufficient qualitative and quantitative consistency in the position, magnitude and width of the major resonant features of n'', including the important spectral band of negative refraction. Therefore, this result ensures the correct choice of the branch in the general retrieval scheme.

For the calculation of the local-field enhancement, two different numerical simulations were performed. First we calculated the process of stimulated emission in a bulk layer of dye without metal and the electric field, $\mathbf{E}_b$, in a unit cell with the same volume, V_Σ, as the volume of the unit cell in our fishnet structure (air and the substrate are excluded). The total power radiated from the bulk layer was calculated as $Q_b = (1/2)\varepsilon_0\omega \int_{V_\Sigma} \varepsilon''|\mathbf{E}_b|^2\, dV_\Sigma$. In the second calculation, the electric field distribution, $\mathbf{E}_f$, was obtained in the fishnet structure using the same conditions as in our pump–probe experiment. The total generated/absorbed power in the fishnet layer is then calculated as $Q_f = (1/2)\varepsilon_0\omega \int_{V_\Sigma} \varepsilon''|\mathbf{E}_f|^2\, dV_\Sigma$. Finally, the enhancement factor was calculated as $\rho = Q_f/Q_b$. It turned out that

©2010 Macmillan Publishers Limited. All rights reserved

the enhancement factor was $\rho = 45$; that is, the total power produced by the gain medium (and absorbed by the nanostructured metal) in the fishnet unit cell was about 45 times larger than that produced by a homogeneous gain material of the same volume.

31. Cai, W. *et al.* Metamagnetics with rainbow colors. *Opt. Exp.* **15,** 3333–3341 (2007).
32. Ku, Z., Dani, K. M., Upadhya, P. C. & Brueck, S. R. Bianisotropic negative-index metamaterial embedded in a symmetric medium. *J. Opt. Soc. Am. B* **26,** B34–B38 (2009).
33. Jackson, J. D. *Classical Electrodynamics* Ch. 7.10 (Wiley, 1975).
34. Cook, J. J. H., Tsakmakidis, K. L. & Hess, O. Ultralow-loss optical diamagnetism in silver nanoforests. *J. Opt. A* **11,** 114026 (2009).
35. Kildishev, A. V. *et al.* Negative refractive index in optics of metal-dielectric composites. *J. Opt. Soc. Am. B* **23,** 423–433 (2006).

©2010 **Macmillan Publishers Limited. All rights reserved**